Pengling Ren
Department of Bioengineering,
Clemson University,
Clemson, SC 29425;
Department of Orthopaedics and Physical Medicine,
Medical University of South Carolina (MUSC),
Charleston, SC 29425;
Department of Radiology,
Beijing Friendship Hospital,
Capital Medical University,
Beijing 100052, China;
Key Laboratory for Biomechanics and Mechanobiology of Ministry of Education,
School of Biological Science and Medical Engineering,
Beihang University,
Beijing 100191, China

Peng Chen
Department of Bioengineering,
Clemson University,
Clemson, SC 29425

Russell A. Reeves
Department of Radiology,
Sidney Kimmel Medical College,
Thomas Jefferson University,
Philadelphia, PA 19107

Nathan Buchweitz
Department of Bioengineering,
Clemson University,
Clemson, SC 29425

Haijun Niu
Key Laboratory for Biomechanics and Mechanobiology of Ministry of Education,
School of Biological Science and Medical Engineering,
Beihang University,
Beijing 100191, China

He Gong
Key Laboratory for Biomechanics and Mechanobiology of Ministry of Education,
School of Biological Science and Medical Engineering,
Beihang University,
Beijing 100191, China

Jeremy Mercuri
Department of Bioengineering,
Clemson University,
Clemson, SC 29425

Charles A. Reitman
Department of Orthopaedics and Physical Medicine,
Medical University of South Carolina (MUSC),
Charleston, SC 29425

Diffusivity of Human Cartilage Endplates in Healthy and Degenerated Intervertebral Disks

The cartilage endplates (CEPs) on the superior and inferior surfaces of the intervertebral disk (IVD), are the primary nutrient transport pathways between the disk and the vertebral body. Passive diffusion is responsible for transporting small nutrient and metabolite molecules through the avascular CEPs. The baseline solute diffusivities in healthy CEPs have been previously studied, however alterations in CEP diffusion associated with IVD degeneration remain unclear. This study aimed to quantitatively compare the solute diffusion in healthy and degenerated human CEPs using a fluorescence recovery after photobleaching (FRAP) approach. Seven healthy CEPs and 22 degenerated CEPs were collected from five fresh-frozen human cadaveric spines and 17 patients undergoing spine fusion surgery, respectively. The sodium fluorescein diffusivities in CEP radial and vertical directions were measured using the FRAP method. The CEP calcification level was evaluated by measuring the average X-ray attenuation. No difference was found in solute diffusivities between radial and axial directions in healthy and degenerated CEPs. Compared to healthy CEPs, the average solute diffusivity was 44% lower in degenerated CEPs (Healthy: 29.07 $\mu m^2/s$ (CI: 23.96–33.62 $\mu m^2/s$); degenerated: 16.32 $\mu m^2/s$ (CI: 13.84–18.84 $\mu m^2/s$), $p < 0.001$). The average solute diffusivity had an inverse relationship with the degree of CEP calcification as determined by the normalized X-ray attenuation values ($\beta = -22.19$, $R^2 = 0.633$; $p < 0.001$). This study suggests that solute diffusion through the disk and vertebral body interface is significantly hindered by CEP calcification, providing clues to help further understand the mechanism of IVD degeneration.
[DOI: 10.1115/1.4056871]

Keywords: intervertebral disk, cartilage endplate, diffusivity, diffusion tensor, fluorescence recovery after photobleaching (FRAP), calcification

[1]Corresponding author.
Manuscript received November 20, 2022; final manuscript received January 29, 2023; published online March 28, 2023. Assoc. Editor: Francesco Travascio.

Hai Yao
Department of Bioengineering,
Clemson University,
Clemson, SC 29425;
Department of Orthopaedics and
Physical Medicine,
Medical University of South Carolina (MUSC),
Charleston, SC 29425

Yongren Wu
Department of Bioengineering,
Clemson University,
68 President Street, MSC501,
Clemson, SC 29425;
Department of Orthopaedics and
Physical Medicine,
Medical University of South Carolina (MUSC),
Charleston, SC 29425
e-mail: yongren@clemson.edu

1 Introduction

Although the specific cause of low back pain remains unclear, symptoms have been strongly associated with intervertebral disk (IVD) degeneration [1–4]. The human IVD includes three parts: cartilage endplate (CEP), annulus fibrosus (AF), and nucleus pulposus (NP). The CEP is a thin hyaline cartilage layer, 500–1500 μm in thickness, present on the superior or inferior surface of the IVD, and acts as the primary transport pathway between the vertebral body and the avascular disk for nutrient and metabolic waste exchange [5–11]. Compared to other disk components (AF and NP), the relatively lower solute diffusivity in healthy CEP leads to a delicate nutrient environment in human IVD (e.g., hypoxia and low glucose level in the central disk region; steep nutrient gradient across the central disk region and boundaries due to the balance of nutrient supply, metabolic waste depletion, and cellular energy metabolism) [8,12,13]. Because of the reliance on nutrient delivery via the CEP, it is generally believed that attenuated nutrient supply due to CEP pathological remodeling (e.g., calcification) may result in impaired extracellular nutrient environment and breakdown of anabolic–catabolic balance in the disk, resulting in cell death, inflammatory response, and disk degeneration progression [10,14–20].

Given the avascular nature of CEP, diffusion is the primary molecular transport mechanism for small nutrients and metabolite solutes [14,16,21]. The solute diffusion rate (i.e., diffusivity) in the cartilaginous tissue is governed by the solute size, composition, and structure of the extracellular matrix [8,9,22–24]. Previous studies have developed electrical conductivity methods to measure the ion (e.g., K^+ and Cl^-) diffusivities in healthy CEP and other disk tissues (AF or NP) [9,25]. The regional and strain-dependent glucose and lactate diffusivities in healthy CEP and AF have been characterized using a diffusion chamber method [8,26]. However, due to the relative scarcity of intact human cadaveric degenerated disk specimens and the typically small, thin, and irregular shapes of surgical degenerated CEP specimens (surgical waste from the spine fusion surgery), the CEP diffusion properties in degenerated disk remain unclear. In addition, since it is difficult to measure the diffusivity in the radial direction due to the small thickness of the CEP in the saggital/coronal plane, the prior CEP diffusivity measurements using the conductivity or diffusion chamber focused on the direction of the vertebral axis (craniocaudal), and neglected to investigate the potential diffusion anisotropy as reported in other cartilaginous tissues and disk components (e.g., articular cartilage, AF) [8,22,23,27].

In contrast to the traditional diffusion measurement methods (e.g., diffusion chamber, radiotracer, magnetic resonance imaging), fluorescence recovery after photobleaching (FRAP) has emerged as a powerful microscopy-based technique for diffusion measurement in the biological tissues or biomaterials [22,23,28,29]: (1) FRAP has a high spatial resolution, permitting diffusion measurements in small regions (e.g., 387.5 μm $\times$ 387.5 μm (128 $\times$ 128 pixels) in this study), making it an ideal method to measure the CEP's diffusion properties, especially in the setting of degenerated and irregular surgical specimens; (2) FRAP can be used to accurately measure the diffusivities in different directions, thereby allowing the identification of diffusion anisotropy. Leveraging the FRAP technique, the objective of this study was to quantitatively characterize the diffusion properties of human CEPs (i.e., diffusion tensor) in healthy and degenerated disks, with the hypothesis that CEP calcification may result in significant decrease in solute diffusivities at both axial and radial directions. The degree of CEP calcification was approximated by measuring X-ray attenuation of the CEPs then further correlated with CEP diffusivity. Histology staining and scanning electron microscopy (SEM) were used to evaluate for CEP microstructure differences between healthy and degenerated IVDs.

2 Materials and Methods

2.1 Specimen Preparation. Seven healthy disks were obtained from five (3/5 (60%) male; 35 $\pm$ 5.5 years old) fresh-frozen cadaveric spines provided by a local Organ Procurement Organization (We Are Sharing Hope SC (SHSC), Charleston, SC). Cadaveric healthy disks were obtained from the L3-4 (4/7 (57%)) and L4-5 (3/7 (43%)) levels; only healthy disks without gross anatomic defects, such as fissures and macrocalcification, were included. Twenty-two degenerated disks were collected as the surgical wastes from 17 patients (10/17 (59%) male; 54 $\pm$ 15.8 years old) undergoing one- or two-level transforaminal lumbar interbody fusion surgery to alleviate disabling low back pain at Medical University of South Carolina (MUSC), with institutional review board approval. Degenerated disks were obtained from the L2-L3 (1/22 (5%)), L3–L4 (5/22 (23%)), L4–L5 (10/22 (45%)), and L5-S1 (6/22 (27%)) levels. Due to the scarcity of human specimens, the effect of disk level was neglected. Disk degeneration was graded by our clinical collaborator (C. R.) based on the Thompson grading system [30]. Degenerated disks obtained following lumbar spine fusion were included if they were Thompson grades III or IV, and healthy cadaveric disks were included if they were grades I or II; intervertebral disks with grade V degeneration were excluded since the diffusion in these specimens would be increased solely due to the presence of macroscopic cracks in the CEP.

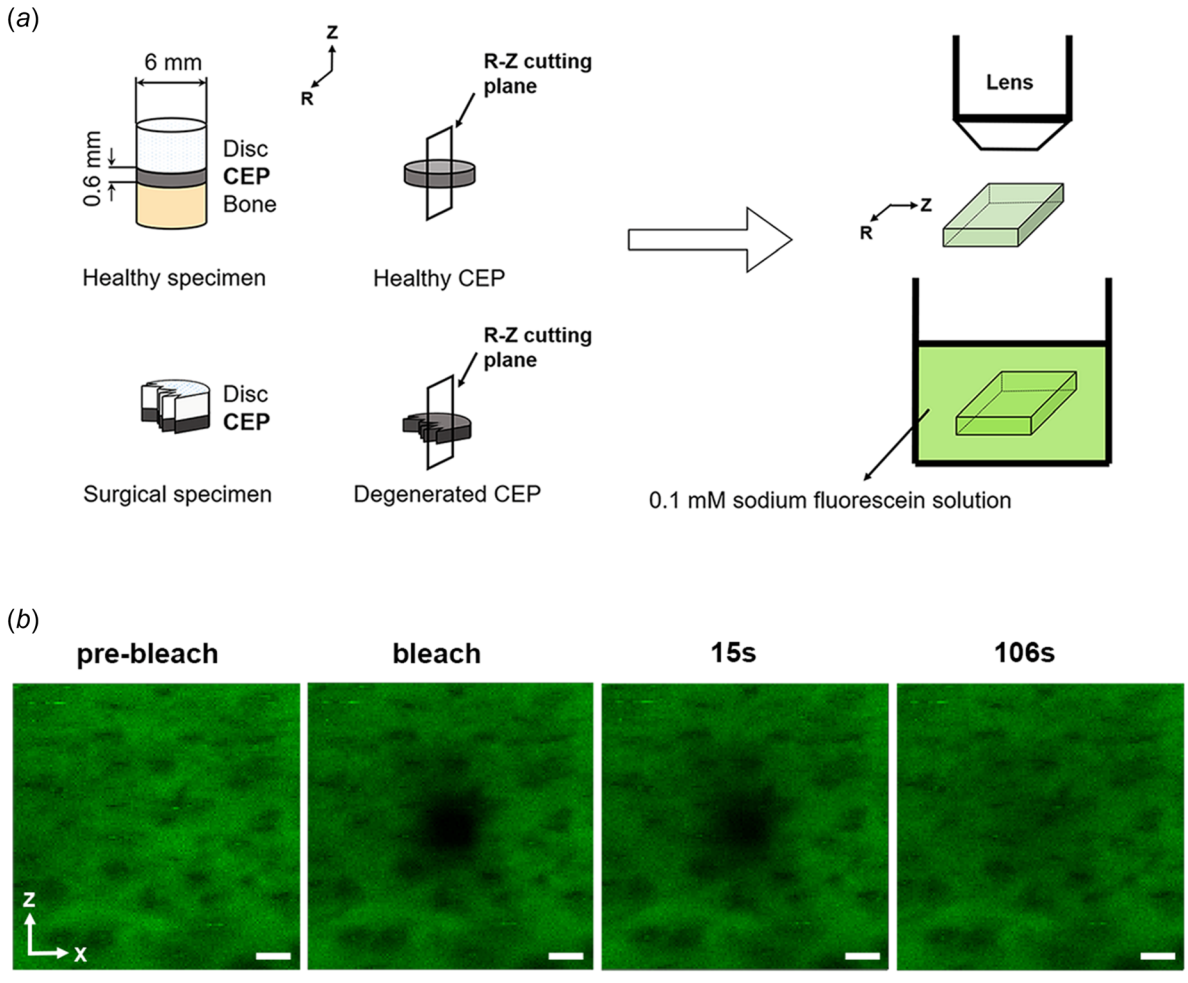

Fig. 1 Schematic of specimen preparation and testing protocols. (*a*) Schematic of specimen preparation. (*b*) Time-series of FRAP measurements including prebleaching, bleaching, and 106 s postbleaching events. Scale bars represent a length of 50 μm. Note: CEP represents cartilage endplate. Radial (*r*) and axial (*z*) directions are parallel and perpendicular to vertebral body, respectively.

The CEPs from the healthy cadaveric disks were prepared by obtaining tissue plugs containing bone, CEP, and NP from the healthy disks; plugs were created with a 5 mm diameter corneal trephine. The specimen preparations were conducted in a moisturized hood to prevent dehydration. The overlying nucleus pulposus, annulus fibrosus, and vertebral bone were subsequently removed from the plugs using a freezing stage microtome (SM2400, Leica Microsystems GmbH, Wetzlar, Germany; Fig. 1(*a*)). The CEPs from the surgical degenerated disks at NP region were prepared using the Leica freezing stage microtome to remove extra disk or bone attachments from the endplates (Fig. 1(*a*)). The average height of the CEP samples is 0.5–0.8 mm, similar to previous studies [8,9]. Due to the thin structure of the CEP specimens, and reservation of even more thinly sliced sections of surgical tissue for diffusivity measurement, the water content could not be reported as done in prior studies [8,31].

2.2 Diffusivity Measurements Using Fluorescence Recovery After Photobleaching. Cartilage endplate specimens were sectioned perpendicular to the axial plane into 100 μm slices using a cryostat across the entire specimen (CM1510S, Leica Microsystems GmbH, Wetzlar, Germany). CEP sections were then immersed in phosphate-buffered saline (PBS) solution with 0.1 mM sodium fluorescein (376 Da) at room temperature (22 °C) for 10 h. The PBS solution's osmolality was adjusted to 400 mM using sodium chloride to prevent tissue swelling [32]. Then the sample was placed in a thin well chamber made by attaching a layer of double-sided adhesive spacer (9 mm in diameter and 0.1 mm in thickness, Secure-Seal spacers, Life Technologies, Grand Island, NY) on a microscope slide (Fig. 1(*a*)). The chamber was sealed with a coverslip. FRAP was performed with a Leica SP5 confocal microscope (Leica Microsystems, Inc., Exton, PA) using a 488 nm Argon laser with a HC PLAN APO 20×/0.7 NA dry objective (Leica Microsystems, Inc., Exton, PA; Fig. 1(*a*)) [28]. The size of the squared bleaching region was set to an area of 48.4 μm × 48.4 μm. A multilayer bleaching protocol was used to ensure two-dimensional fluorescent recovery by minimizing the diffusion along the optical axis. Fluorescence recovery was measured at a depth of 7 μm beneath the surface of the specimen. For each FRAP measurement, five images on bleaching region of interest (387.5 μm × 387.5 μm (128 × 128 pixels)) were obtained prior to photobleaching and 200 images with the same size were acquired postbleaching at a scanning rate of either 0.358 s or 0.713 s per frame. Background sample fluorescence was removed by subtracting the average pixel value of the prebleaching images from the postbleaching images. A total of 2–5 FRAP diffusivity measurements were taken per CEP slice and 2–4 slices were obtained per disk. A previously developed fluorescent image postprocessing MATLAB program was utilized to calculate the two-dimensional diffusion tensor in CEPs based on previously developed spatial Fourier analysis: this included solute diffusivities in the radial (D_{rr}) and axial (D_{zz}) directions and average diffusivity ($D_{\text{Average}} = (D_{rr} + D_{zz})/2$] [22,23,28].

2.3 Morphologic Assessment of the Cartilage Endplate Using Histology and Scanning Electron Microscopy. Histologic analysis of the CEPs was performed by taking tissue plugs

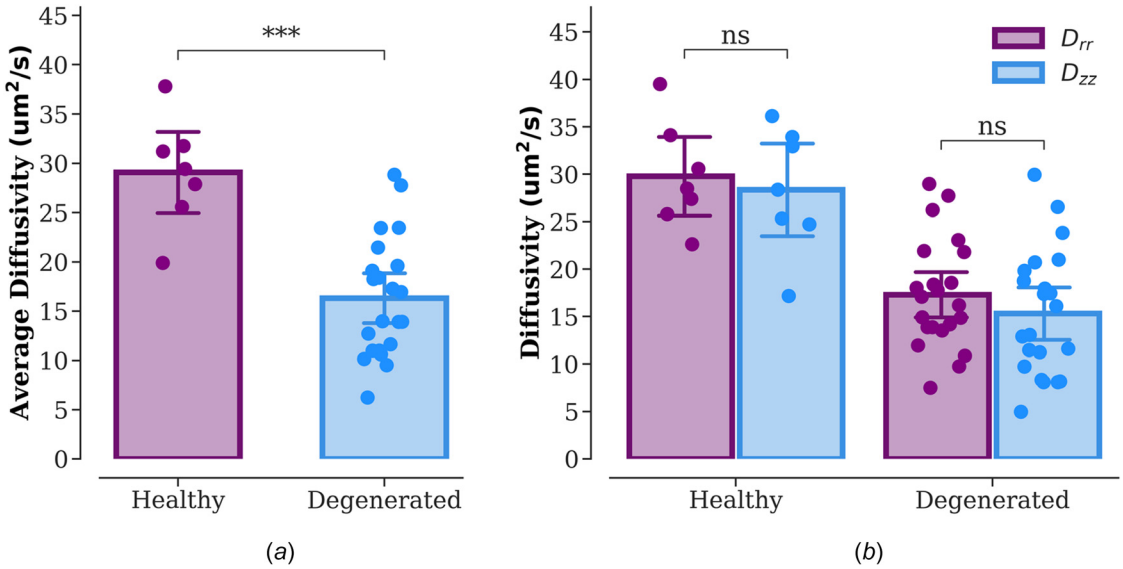

Fig. 2 Solute diffusivities in CEPs from healthy ($n = 7$) and degenerated ($n = 22$) groups. (*a*) Average diffusivity ($D_{Average} = (D_{rr} + D_{zz})/2$). (*b*) Diffusivities in the radial (D_{rr}) and axial (D_{zz}) directions. Note: $^{***}p < 0.001$; NS: no significant difference. The scale bar represents 95% CI.

containing vertebral bone, CEP, and NP from healthy ($n = 3$) and degenerated disks ($n = 3$) and fixing them at room temperature in 10% neutral buffered formalin for 2 days, followed by ethylenediaminetetraacetic acid decalcification for 2 weeks and embedding in paraffin wax [8,24]. The CEPs were then cut into 6 μm thick sections and stained using a combination of Safranin-O and Fast Green dyes; this stains proteoglycans varying shades of red and noncollagenous proteins green. Microscopic images were captured at 4× magnification (Olympus BX51, Olympus Scientific Solutions, Waltham, MA). SEM of the CEPs was performed by fixing CEP sections (healthy CEPs: $n = 3$; degenerated CEPs: $n = 3$) in a solution of 2.5% glutaraldehyde in PBS at 4 °C for 48 h. The fixed tissues were subsequently dehydrated using a graded series of ethanol (50%, 70%, 90%, and 100% *v*/*v* ethanol in water). The specimens were then further dried by immersion in hexamethyldisilazane. The samples were coated with a 20 nm thick layer of gold to enhance SEM image contrast. SEM images were obtained at 3000× magnification (Hitachi TM-1000, Hitachi High-Tech America, Inc., Schaumburg, IL).

2.4 Evaluating Cartilage Endplate Calcification Using X-Ray. X-ray images of the CEP specimen were obtained using a digital Faxitron DX X-ray cabinet (Faxitron Bioptics, LLC, Tucson, AZ) at 10 mAs, 25 kVp. Images were acquired from the CEP specimens (CEP radial direction in parallel to the surface of the X-ray image detector). A region of interest was drawn on the diffusion sampling area and the average grayscale pixel value of each CEP was recorded; this average grayscale pixel value was used as a surrogate for quantifying endplate calcification, specifically, those with higher average grayscale pixel intensities having more endplate calcification than samples with lower average grayscale pixel intensity. The average grayscale pixel intensity was then normalized from 0.0 to 1.0 by subtracting the minimum average grayscale measurement from each sample and then dividing by the range of average grayscales (i.e., maximum average grayscale measurement–minimum average grayscale measurement). X-ray quantification and analysis were performed by two members (R. R. and P. R.) who were blinded to patient demographics and whether the sample was obtained from a surgical specimen or from a cadaver.

2.5 Statistical Analysis. Diffusivity measurements were repeated multiple times per CEP tissue section slice (technical replicates) in order to increase the precision in the measured diffusivity (317 diffusivity measurements in total, 2–5 (four on average) replicates per CEP slice); the distributions of these technical replicates were later assessed for normality using the Shapiro–Wilk test and several of the distributions were noted to significantly deviate from normality. As such, we chose to record the median of these technical replicates rather than their averages. Multiple CEP tissue section slices (78 CEP section slices in total from 29 disks (2.7 slices on average per IVD)) were also obtained from each unique IVD (biological replicates) in order to account for biological variation in diffusivity based on minor differences in anatomic location within the IVD; the median diffusivity was then again obtained across the biological replicates to obtain the final radial and axial diffusivity measurements per IVD (healthy disks: $n = 7$; degenerated disks: $n = 22$).

Differences in the median diffusivity, herein referred to simply as diffusivity, within the CEPs were examined using two-way ANOVA, assessing for differences based on diffusion directionality (radial and axial directions) and degeneration status (cadaveric healthy versus surgical degenerated specimen). Furthermore, effect of degeneration status on the average diffusivity (average of the final radial and axial diffusivities in each disk ($D_{Average} = (D_{rr} + D_{zz})/2$)) was examined using student's t-test. The relationship between average CEP diffusivity and the degree of tissue calcification, as assessed by normalized X-ray attenuation values, was assessed using linear regression. Due to sample size limitations, the effects of sex, age, and disk level could not be evaluated. All statistical analyses were performed using IBM SPSS Statistics for Windows, Version 27.0, released 2020 (IBM Corp., Armonk, NY). Differences in significant main effects are reported as mean diffusivity with the 95% confidence interval (CI), obtained using a bias corrected accelerated bootstrapping technique. Observed power was reported for nonstatistically significant differences. *P*-values less than 0.05 were considered statistically significant.

3 Results

3.1 Solute Diffusivities. The average diffusivity ($D_{Average}$) was significantly higher in CEPs from the healthy group than degenerated group (Healthy: 29.07 $\mu m^2/s$ (CI: 23.96–33.62 $\mu m^2/s$); Degenerated: 16.32 $\mu m^2/s$ (CI: 13.84–18.84 $\mu m^2/s$), $p < 0.001$, Fig. 2(*a*)). Additionally, there was no main effect of directionality (radial versus axial directions) on sodium

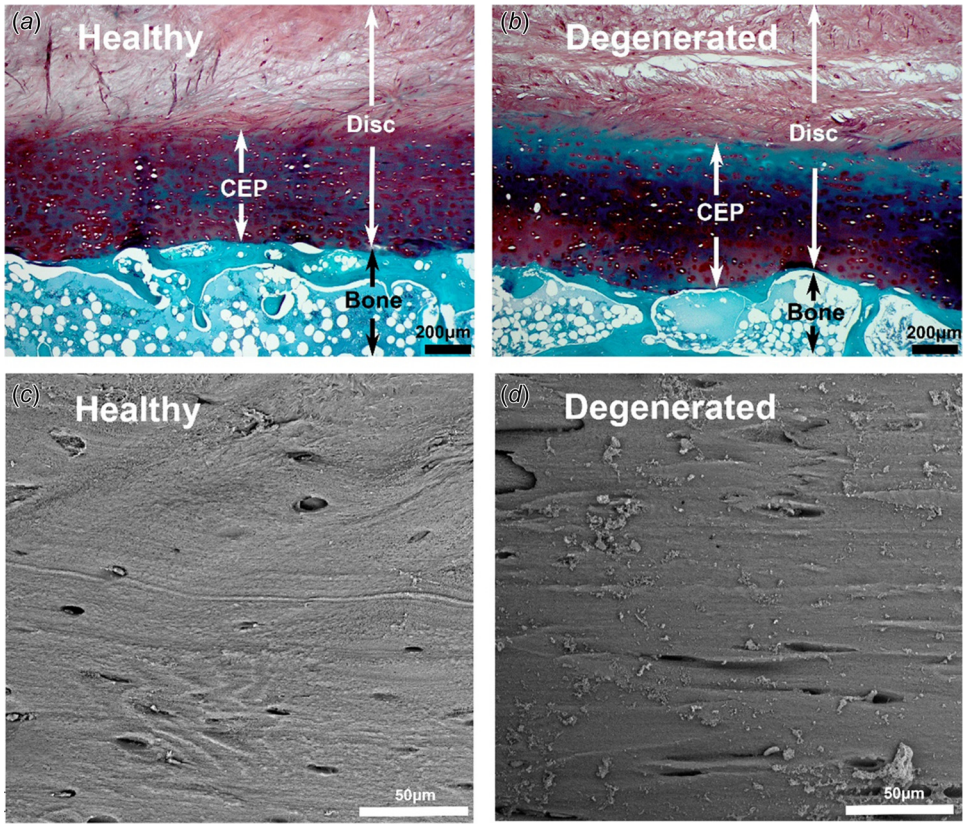

Fig. 3 Histological images of disk and bone interfaces ((*a*) and (*b*)) and SEM images of CEP regions ((*c*) and (*d*)) from healthy and degenerated groups

fluorescein diffusivities ($p = 0.372$; Fig. 2(*b*)); however, the observed power of this finding was only 14.3%. Similarly, there was no two-way interaction between diffusion directionality (radial (D_{rr}) versus axial (D_{zz}) directions) and the presence of IVD degeneration (cadaveric versus surgical specimen; $p = 0.372$); although, the observed power of this finding was only 5.3%.

3.2 Histological Appearance and Microstructure. Histological images showed a thin CEP at the interface between the vertebral body and NP in healthy and degenerated groups (Fig. 3). The healthy samples exhibited the normal CEP transition pattern with abundant proteoglycan (red stain) and compact collagen fiber structure (Fig. 3(*a*), CEP). However, samples from degenerated disks demonstrated lower levels of proteoglycan in CEP region including an acellular dark blue band, which indicated tissue calcification and necrosis (Fig. 3(*b*)). SEM images further demonstrated the usual lamellated collagen fiber structure of the CEP in healthy samples (Fig. 3(*c*)), while the CEPs in degenerated IVDs showed a slightly more compact collagen structure (Fig. 3(*d*)).

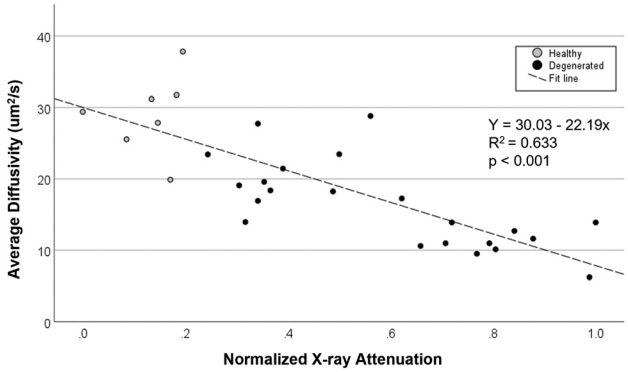

Fig. 4 Correlation between average diffusivity and CEP calcification level, as assessed by the normalized average CEP X-ray attenuation. Gray dots and black dots indicate the cartilage endplates from healthy ($n = 7$) and degenerated ($n = 22$) groups, respectively.

3.3 Correlation Between Diffusivity and Cartilage Endplate Calcification. There was a strong inverse correlation between mean CEP diffusivity and CEP calcification, as measured by the mean normalized X-ray attenuation (Fig. 4). A linear regression was calculated to predict CEP diffusivity based on the degree of normalized X-ray attenuation by the CEP. A significant regression equation was found ($F(1, 27) = 46.516$, $p < 0.001$), with an R^2 of 0.633 and β of −22.19 (95% CI −27.58 to −17.50). Predicted CEP diffusivity is equal to $30.03 - (22.19 \times (\text{X-ray attenuation}))$ $\mu m^2/s$ when the average X-ray attenuation is corrected to a 0.0 to 1.0 scale. CEP diffusivity decreased by 2.219 $\mu m^2/s$ for each 0.1 unit increase in X-ray attenuation.

4 Discussion

This study used a FRAP technique to quantify the axial and radial sodium fluorescein diffusivities in CEPs from healthy and degenerated human IVDs. These quantitative measurements allow the investigation on, to which extent as a potential indicator of nutrient supply deficiency, the CEP calcification would alter the solute diffusion to the IVD, providing clues to help further understand the mechanism of IVD degeneration. Specifically, the diffusivity in healthy CEPs is approximately 10% (versus inner axial direction) and 76% (versus outer radial direction) of that in healthy human AF, respectively (Table 1) [5,22]. This comparison supports the previous notion that, the healthy CEP layers can

Table 1 The diffusivities (mean (CI)) of different solutes in various cartilaginous tissues (CEP: cartilage endplate; AF: annulus fibrosus; AC: articular cartilage; TMJ disk: temporomandibular joint disk)

Specimens	Type of solute	Diffusivities ($\mu m^2/s$)	References
Human CEP	Sodium fluorescein (376 Da)	29.1 (25.8–32.4) (healthy; average) 16.3 (14.5–18.2) (degenerated; average)	Present Study
Human CEP	Sodium fluorescein (376 Da)	5.9–21.5 (healthy; average)	[6]
Human CEP	Glucose (180 Da)	24.7–44.1 (healthy; axial)	[8]
Human CEP	Glucose (180 Da)	18–58 (healthy; axial)	[5]
Human AF	Glucose (180 Da)	170 (axial)	[5]
Human AF	Fluorescein (332 Da)	104–268 (axial) 38–119 (radial)	[22]
Human AC	Glucose (180 Da)	135–146 (axial)	[27]
Human AC	Fluorescein (332 Da)	114.1 (81.5–146.7) (femur; average) 107.8 (81.7–133.9) (tibia; average)	[33]
Human meniscus	Fluorescein (332 Da)	56.5 (24.9–88.1) (radial) 106.3 (46.7–165.9) (circumferential)	[34]
Porcine meniscus	Fluorescein (332 Da)	84.4 (50.5–118.3) (average)	[35]
Porcine TMJ disk	Fluorescein (332 Da)	57.0 (43.0–71.0) (average)	[23]

block rapid nutrient/metabolite solute exchange between the disk and its surrounding environment, and help to maintain a delicate and stable extracellular nutrient environment, especially the nutrient gradients from the peripheral edge to central region of the disk (with low oxygen and glucose levels in the central region) [8,9,16,31]. Furthermore, the CEP diffusivity in degenerated disk was approximately 44% lower compared to that in healthy disk. Such a significantly decreased solute diffusivity in CEPs from the degenerated disk suggests a reduced nutrient delivery to and potential nutrient deficiency inside the avascular center portions of the disk, which may trigger a cascade of cellular biological responses to initiate or accelerate the disk degeneration progression [10,14,16,19].

This study demonstrated a strong inverse relationship between CEP diffusivity and the degree of calcification, as assessed by the normalized X-ray attenuation. These findings support the general hypothesis of potential attenuated nutrient solute transport through calcified CEPs during disk degeneration process [6,15,18,20,31]. Additionally, the CEPs from degenerated disks in this study histologically showed a band of overt loss of proteoglycans, tissue calcification, and necrosis. SEM images revealed a relatively more compacted collagen microstructure in CEPs from the degenerated group when compared to healthy group. It indicates that the hindered nutrient diffusion is likely driven by compositional and microscopic structural changes in CEPs, which are consistent with prior studies, specifically that diffusion rates are related to biochemical composition (e.g., calcification, hydration, proteoglycan), and microscopic collagen structure of the matrix [5,24,36–38].

The isotropic sodium fluorescein diffusion pattern in CEPs from both healthy and degenerated disks distinguished this thin layer of hyaline cartilage on the vertebral body-disk interface from other anisotropic cartilaginous tissues, such as the annulus fibrosis, articular cartilage, and the temporomandibular joint [22,28,39]. Interestingly, unlike those tissues with overt fibrous structures, the CEP structure lacks clear fiber arrangement zones and is much more compact (Fig. 3), further supporting the unique isotropic structure-diffusion relationship paradigm in the CEP. Similar isotropic diffusion properties in calcified CEPs from degenerated disks further suggests that CEP calcification resulted in no directional preference for diffusion; however, the absence of these findings could be due to limited statistical power to detect subtle changes.

Due to the technical difficulties of in vivo detection, finite element (FE) analysis has been utilized to predict the extracellular mechano-electrochemical environment in human IVD under various mechanical loading conditions [12,15,40–42]. To improve the accuracy of FE modeling predictions, representative disk material property is one of the key factors. Although the NP and AF have been extensively characterized [5,10,16,22,25,31,43], the experimentally determined constitutive relationships of the human CEP in the IVD and vertebral body interface is rare, especially the extent to which the CEP calcification changes the CEP diffusion properties. Generally, the CEP was either neglected or simplified as a layer of articular cartilage or AF tissue in the FE modeling. Integrating the distinct CEP isotropic calcification-diffusion relationship from health and degenerated disks found in this study and computed tomography or X-ray imaging for in vivo CEP calcification assessment, the image-based FE modeling may help to further understand the impact of CEP calcification or mineralization on the extracellular disk nutrient environment and subsequent IVD degenerative remodeling mechanism.

This study has several limitations. First, the relatively small sample size prohibited accurate characterization of the effects of other factors such as the anatomic disk level, age, and sex. Second, the molecular weight of fluorescein (376 Da) in our study is slightly higher than the molecular weight of critical nutrient solutes such as glucose (180 Da). However, it can still provide insights into the relative changes of the nutrient diffusion in calcified CEPs from the degenerated disks comparing to the healthy CEPs. Third, due to the semidestructive nature of surgical sample harvesting, it is challenging to distinguish the anterior–posterior, and right–left (lateral) directions in surgical specimens. Therefore, we could only evaluate differences in diffusion based on the axial and radial directions. It is possible that there could be differences in diffusion in the anterior–posterior and right–left axes, although no large variation was noted in the radial directions that would suggest such a phenomenon. Fourth, surgical sample measurements were taken in the areas of intact calcification; however, the overall CEP layer in late disk degeneration stages could be fibrotic, ossified, and highly damaged. Future attention is needed on the composite transport properties of the degenerated CEPs. Fifth, the degree of calcification in CEPs was approximated using normalized X-ray attenuation measurements but this is a surrogate measure instead of a direct mineralization assessment. Finally, since the geometry of the surgically harvested CEP samples from degenerated disks was thin and irregularly shaped, it was not possible to measure both diffusivity and biochemical compositions (e.g., proteoglycan, collagen, extracellular matrix porosity) for the endplate. Similarly, since the prior developed diffusivity measurement technique in a confined chamber was unable to be utilized for these surgical CEP samples [8], the strain-dependent diffusivity was also unable to be elucidated. Future larger scale cadaver studies where relatively intact endplate from the degenerative disks are more available could incorporate these measurements.

In summary, (1) the diffusivity in calcified CEPs from degenerated disks was discovered to be 44% lower compared with that in healthy CEPs; (2) an inverse correlation was found between CEP

calcification and solute diffusion; (3) compared to other disk components, a distinct slow and isotropic diffusion pattern of the sodium fluorescein was found in CEPs from both healthy and degenerated IVDs. These findings suggested that, the CEP pathological change (e.g., calcification) could significantly hinder the nutrient diffusion through the disk and vertebral body interface, which may lead to IVD nutrient deficiency and initiate or accelerate the disk degeneration progression.

Acknowledgment

This study was approved by the Institutional Review Board of the Medical University of South Carolina.

Funding Data

- NIH/NIGMS COBRE: South Carolina Translational Research Improving Musculoskeletal Health (SC TRIMH; P20GM121342; Funder ID: 10.13039/100000057).
- Cervical Spine Research Society Seed Starter grant (Funder ID: 10.13039/100002718).

Data Availability Statement

The datasets generated and supporting the findings of this article are obtainable from the corresponding author upon reasonable request.

References

[1] Hartvigsen, J., Hancock, M. J., Kongsted, A., Louw, Q., Ferreira, M. L., Genevay, S., Hoy, D., Karppinen, J., Pransky, G., Sieper, J., Smeets, R. J., and Underwood, M., and Lancet Low Back Pain Series Working Group, 2018, "What Low Back Pain Is and Why We Need to Pay Attention," Lancet, **391**(10137), pp. 2356–2367.

[2] Luoma, K., Riihimaki, H., Luukkonen, R., Raininko, R., Viikari-Juntura, E., and Lamminen, A., 2000, "Low Back Pain in Relation to Lumbar Disc Degeneration," Spine, **25**(4), pp. 487–492.

[3] Munir, S., Freidin, M. B., Rade, M., Maatta, J., Livshits, G., and Williams, F. M. K., 2018, "Endplate Defect Is Heritable, Associated With Low Back Pain and Triggers Intervertebral Disc Degeneration: A Longitudinal Study From TwinsUK," Spine, **43**(21), pp. 1496–1501.

[4] Vlaeyen, J. W. S., Maher, C. G., Wiech, K., Van Zundert, J., Meloto, C. B., Diatchenko, L., Battié, M. C., Goossens, M., Koes, B., and Linton, S. J., 2018, "Low Back Pain," Nat. Rev. Dis. Primers, **4**(1), p. 52.

[5] Maroudas, A., Stockwell, R. A., Nachemson, A., and Urban, J., 1975, "Factors Involved in the Nutrition of the Human Lumbar Intervertebral Disc: Cellularity and Diffusion of Glucose In Vitro," J. Anat., **120**(Pt 1), pp. 113–130.

[6] Wong, J., Sampson, S., Bell-Briones, H., Ouyang, A., Lazar, A., Lotz, J., and Fields, A., 2019, "Nutrient Supply and Nucleus Pulposus Cell Function: Effects of the Transport Properties of the Cartilage Endplate and Potential Implications for Intradiscal Biologic Therapy," Osteoarthritis Cartilage, **27**(6), pp. 956–964.

[7] Ogata, K., and Whiteside, L. A., 1981, "Nutritional Pathways of the Intervertebral Disc: An Experimental Study Using Hydrogen Washout Technique," Spine, **6**(3), pp. 211–216.

[8] Wu, Y., Cisewski, S. E., Wegner, N., Zhao, S., Pellegrini, V. D., Jr., Slate, E. H., and Yao, H., 2016, "Region and Strain-Dependent Diffusivities of Glucose and Lactate in Healthy Human Cartilage Endplate," J. Biomech., **49**(13), pp. 2756–2762.

[9] Wu, Y., Cisewski, S. E., Sun, Y., Damon, B. J., Sachs, B. L., Pellegrini, V. D., Jr., Slate, E. H., and Yao, H., 2017, "Quantifying Baseline Fixed Charge Density in Healthy Human Cartilage Endplate: A Two-Point Electrical Conductivity Method," Spine, **42**(17), pp. E1002–E1009.

[10] DeLucca, J. F., Cortes, D. H., Jacobs, N. T., Vresilovic, E. J., Duncan, R. L., and Elliott, D. M., 2016, "Human Cartilage Endplate Permeability Varies With Degeneration and Intervertebral Disc Site," J. Biomech., **49**(4), pp. 550–557.

[11] Fields, A. J., Rodriguez, D., Gary, K. N., Liebenberg, E. C., and Lotz, J. C., 2014, "Influence of Biochemical Composition on Endplate Cartilage Tensile Properties in the Human Lumbar Spine," J. Orthop. Res., **32**(2), pp. 245–252.

[12] Wu, Y., Cisewski, S., Sachs, B. L., and Yao, H., 2013, "Effect of Cartilage Endplate on Cell Based Disc Regeneration: A Finite Element Analysis," Mol. Cell. Biomech., **10**(2), pp. 159–182.

[13] Huang, Y. C., Urban, J. P., and Luk, K. D., 2014, "Intervertebral Disc Regeneration: Do Nutrients Lead the Way?," Nat. Rev. Rheumatol., **10**(9), pp. 561–566.

[14] Urban, J., Holm, S., Maroudas, A., and Nachemson, A., 1982, "Nutrition of the Intervertebral Disc: Effect of Fluid Flow on Solute Transport," Clin. Orthop. Relat. Res., **170**, pp. 296–302.

[15] Jackson, A. R., Huang, C.-Y. C., Brown, M. D., and Gu, W. Y., 2011, "3D Finite Element Analysis of Nutrient Distributions and Cell Viability in the Intervertebral Disc: Effects of Deformation and Degeneration," ASME J. Biomech. Eng., **133**(9), p. 01006.

[16] Nachemson, A., Lewin, T., Maroudas, A., and Freeman, M., 1970, "In Vitro Diffusion of Dye Through the End-Plates and the Annulus Fibrosus of Human Lumbar Inter-Vertebral Discs," Acta Orthop. Scand., **41**(6), pp. 589–607.

[17] Rajasekaran, S., Babu, J. N., Arun, R., Armstrong, B. R., Shetty, A. P., and Murugan, S., 2004, "A Study of Diffusion in Human Lumbar Discs: A Serial Magnetic Resonance Imaging Study Documenting the Influence of the Endplate on Diffusion in Normal and Degenerate Discs," Spine, **29**(23), pp. 2654–2667.

[18] Roberts, S., Menage, J., and Eisenstein, S., 1993, "The Cartilage Endplate and Intervertebral Disc in Scoliosis: Calcification and Other Sequelae," J. Orthop. Res., **11**(5), pp. 747–757.

[19] Dolor, A., Sampson, S. L., Lazar, A. A., Lotz, J. C., Szoka, F. C., and Fields, A. J., 2019, "Matrix Modification for Enhancing the Transport Properties of the Human Cartilage Endplate to Improve Disc Nutrition," PLoS One, **14**(4), p. e0215218.

[20] Grant, M. P., Epure, L. M., Bokhari, R., Roughley, P., Antoniou, J., and Mwale, F., 2016, "Human Cartilaginous Endplate Degeneration Is Induced by Calcium and the Extracellular Calcium-Sensing Receptor in the Intervertebral Disc," Eur. Cells Mater., **32**, pp. 137–151.

[21] Urban, J., Holm, S., and Maroudas, A., 1978, "Diffusion of Small Solutes Into the Intervertebral Disc: As In Vitro Study," Biorheology, **15**(3–4), pp. 203–223.

[22] Travascio, F., Jackson, A. R., Brown, M. D., and Gu, W. Y., 2009, "Relationship Between Solute Transport Properties and Tissue Morphology in Human Annulus Fibrosus," J. Orthop. Res., **27**(12), pp. 1625–1630.

[23] Shi, C., Wright, G. J., Ex-Lubeskie, C. L., Bradshaw, A. D., and Yao, H., 2013, "Relationship Between Anisotropic Diffusion Properties and Tissue Morphology in Porcine TMJ Disc," Osteoarthritis Cartilage, **21**(4), pp. 625–633.

[24] Wu, Y., Cisewski, S. E., Sachs, B. L., Pellegrini, V. D., Jr., Kern, M. J., Slate, E. H., and Yao, H., 2015, "The Region-Dependent Biomechanical and Biochemical Properties of Bovine Cartilaginous Endplate," J. Biomech., **48**(12), pp. 3185–3191.

[25] Jackson, A. R., Travascio, F., and Gu, W. Y., 2009, "Effect of Mechanical Loading on Electrical Conductivity in Human Intervertebral Disk," ASME J. Biomech. Eng., **131**(5), p. 054505.

[26] Jackson, A. R., Yuan, T. Y., Huang, C. Y., Travascio, F., and Yong Gu, W., 2008, "Effect of Compression and Anisotropy on the Diffusion of Glucose in Annulus Fibrosus," Spine, **33**(1), pp. 1–7.

[27] Maroudas, A., 1970, "Distribution and Diffusion of Solutes in Articular Cartilage," Biophys. J., **10**(5), pp. 365–379.

[28] Shi, C., Kuo, J., Bell, P. D., and Yao, H., 2010, "Anisotropic Solute Diffusion Tensor in Porcine TMJ Discs Measured by FRAP With Spatial Fourier Analysis," Ann. Biomed. Eng., **38**(11), pp. 3398–3408.

[29] Chen, P., Chen, X., Hepfer, R. G., Damon, B. J., Shi, C., Yao, J. J., Coombs, M. C., Kern, M. J., Ye, T., and Yao, H., 2021, "A Noninvasive Fluorescence Imaging-Based Platform Measures 3D Anisotropic Extracellular Diffusion," Nat. Commun., **12**(1), p. 1913.

[30] Thompson, J. P., Pearce, R. H., Schechter, M. T., Adams, M. E., Tsang, I. K., and Bishop, P. B., 1990, "Preliminary Evaluation of a Scheme for Grading the Gross Morphology of the Human Intervertebral Disc," Spine, **15**(5), pp. 411–415.

[31] Roberts, S., Urban, J. P., Evans, H., and Eisenstein, S. M., 1996, "Transport Properties of the Human Cartilage Endplate in Relation to Its Composition and Calcification," Spine, **21**(4), pp. 415–420.

[32] Spillekom, S., Smolders, L. A., Grinwis, G. C., Arkesteijn, I. T., Ito, K., Meij, B. P., and Tryfonidou, M. A., 2014, "Increased Osmolarity and Cell Clustering Preserve Canine Notochordal Cell Phenotype in Culture," Tissue Eng., Part C, **20**(8), pp. 652–662.

[33] Travascio, F., Valladares-Prieto, S., and Jackson, A. R., 2020, "Effects of Solute Size and Tissue Composition on Molecular and Macromolecular Diffusivity in Human Knee Cartilage," Osteoarthritis Cartilage Open, **2**(4), p. 100087.

[34] Travascio, F., Devaux, F., Volz, M., and Jackson, A. R., 2020, "Molecular and Macromolecular Diffusion in Human Meniscus: Relationships With Tissue Structure and Composition," Osteoarthritis Cartilage, **28**(3), pp. 375–382.

[35] Schwartz, G., Morejon, A., Best, T. M., Jackson, A. R., and Travascio, F., 2022, "Strain-Dependent Diffusivity of Small and Large Molecules in Meniscus," ASME J. Biomech. Eng., **144**(11), p. 111010.

[36] Burstein, D., Gray, M. L., Hartman, A. L., Gipe, R., and Foy, B. D., 1993, "Diffusion of Small Solutes in Cartilage as Measured by Nuclear Magnetic Resonance (NMR) Spectroscopy and Imaging," J. Orthop. Res., **11**(4), pp. 465–478.

[37] Gu, W. Y., Yao, H., Huang, C. Y., and Cheung, H. S., 2003, "New Insight Into Deformation-Dependent Hydraulic Permeability of Gels and Cartilage, and Dynamic Behavior of Agarose Gels in Confined Compression," J. Biomech., **36**(4), pp. 593–598.

[38] Gu, W. Y., and Yao, H., 2003, "Effects of Hydration and Fixed Charge Density on Fluid Transport in Charged Hydrated Soft Tissues," Ann. Biomed. Eng., **31**(10), pp. 1162–1170.

[39] Jackson, A. R., and Gu, W. Y., 2009, "Transport Properties of Cartilaginous Tissues," Curr. Rheumatol. Rev., **5**(1), pp. 40–50.
[40] Shirazi-Adl, A., Taheri, M., and Urban, J. P., 2010, "Analysis of Cell Viability in Intervertebral Disc: Effect of Endplate Permeability on Cell Population," J. Biomech., **43**(7), pp. 1330–1336.
[41] Soukane, D. M., Shirazi-Adl, A., and Urban, J. P., 2007, "Computation of Coupled Diffusion of Oxygen, Glucose and Lactic Acid in an Intervertebral Disc," J. Biomech., **40**(12), pp. 2645–2654.
[42] Huang, C. Y., and Gu, W. Y., 2008, "Effects of Mechanical Compression on Metabolism and Distribution of Oxygen and Lactate in Intervertebral Disc," J. Biomech., **41**(6), pp. 1184–1196.
[43] Gu, W. Y., Mao, X. G., Rawlins, B. A., Iatridis, J. C., Foster, R. J., Sun, D. N., Weidenbaum, M., and Mow, V. C., 1999, "Streaming Potential of Human Lumbar Anulus Fibrosus Is Anisotropic and Affected by Disc Degeneration," J. Biomech., **32**(11), pp. 1177–1182.